COMPUTER-AIDED DESIGN & APPLICATIONS, 2015
VOL. 12, NO. S1, 33–47
http://dx.doi.org/10.1080/16864360.2015.1077073

Topological optimization of automotive structures under impact using robust design

Augusto Millán Gardea and José Carlos Miranda Valenzuela

Tecnológico de Monterrey, Campus Toluca, Automotive Engineering Research Center

ABSTRACT

Structure optimization has been widely used within automotive applications. Lighter structures are needed due to their favorable influence on fuel economy, power requirements, top speed, among many other factors. On the other hand, stiff, strong and stable structures are also essential due to how these favor the static and dynamic behavior of the vehicle as well as the safety conditions for the occupants.

Previously mentioned properties tend to be oppositely related, reason why optimization is indispensable. In this work the collapse region of a light chassis is optimized using robust design techniques.

With the intention of maximizing energy absorption, the number, size and position of collapse triggers are determined considering factors that influence a collision in real-life situations, and cannot be controlled. Such factors include the vertical and horizontal angles of impact as well as variations in the thickness of the material used to manufacture the chassis.

From the obtained results, the amount of energy absorbed by the chassis, in non-perfect frontal impacts, can be enhanced using multiple triggers positioned along its collapsible region.

KEYWORDS

Topological optimization; impact; robust design; automotive structure

1. Introduction

In automotive engineering, design and manufacture, there has always been a constant concern about safety. Despite the continuous development of safety mechanisms and the exponential growth of technology focused on this same aspect, nowadays, the amount of traffic accidents with tragic consequences is still of alarming proportions. According to the World Health Organization, around 1.23 million people loose their lives in car accidents annually [21]. This may be caused by design, material or device deficiencies, or by lack of awareness or expertise in the user. Nevertheless as the latter is outside the control of automotive engineers, it is of prime importance to focus our efforts on providing the user with the safest possible vehicle, this, without compromising other functions and even counteracting human deficiencies with intelligent systems.

From the structural point of view, the most important part of a vehicle is its chassis, providing most of the stiffness, being crucial for the safety of the occupants and granting the foundation for other systems, which makes it the best candidate component to optimize [13]. This work focuses on the optimization of the collapsible region from a lightweight chassis in order to provide the maximum amount of absorbed energy, through minimizing the influence of external factors, such as impact angles, that commonly occur in everyday traffic accidents. In this regards, it is recognized that frontal impacts in vehicles rarely are perfect in nature, meaning that in most cases the driver reacts to the imminent impact by braking and/or steering. As a consequence, the vehicle, and therefore its chassis, deviates from the frontal impact perfect condition, which is commonly considered in crashworthiness analysis. As the impact is no longer perfectly perpendicular to the chassis, the energy absorption properties of the structure are affected.

Starting from a previously designed chassis, an optimization methodology is created for its use on lightweight chassis, without compromising functionality and focusing on its performance during imperfect collisions, predominantly involving Computer Assisted Design (CAD), Computer Assisted Engineering (CAE) and Robust Design techniques.

CONTACT Augusto Millán Gardea augusto.millan@itesm.mx

2. State of the art

As the automotive industry looks for better fuel efficiency and increased safety, the field of structural optimization involving crashworthiness is gaining importance every day. Current research in this field focuses on areas like "topological optimization focused on impact scenarios", "topological optimization using energy absorption as objective function", "optimal design of automotive structures for crashworthiness" and "automotive structures behavior under impact".

In this regard, several authors have used Taguchi's methodologies to improve the performance of structures under impact. Abbasi et al. [1] used the Taguchi method and parametric design optimization to improve the crashworthiness of an automotive body. The thickness of principal internal parts of the automotive frontal crumple zone was employed as design variable for optimization. In another work, Abbasi et al. [2] improved the crashworthiness of an automotive structure using Fuzzy Logic and Taguchi methods.

Also, in terms of topological optimization Christensen [4] optimized the structure of a light hybrid vehicle focusing on crashworthiness, this, through the simultaneous application of 7 different load cases, Forsberg [8] optimizes by determining load routes with a non-sensibility based convergence method, reducing significantly the computational cost, and Schumacher [17] optimizes by implementing "bubbles", starting with ranked CAD parameters, which may be easily modified.

Having an overview of the work already done and finding a potentially unexploited area, the research presented in this work focuses on the implementation of collapse triggers (see Fig. 1), which are geometrical alterations done on a structure, causing it to collapse in an optimal and controlled manner during a collision.

Despite being an uncommonly addressed topic, a previous study about collapse triggers was found.

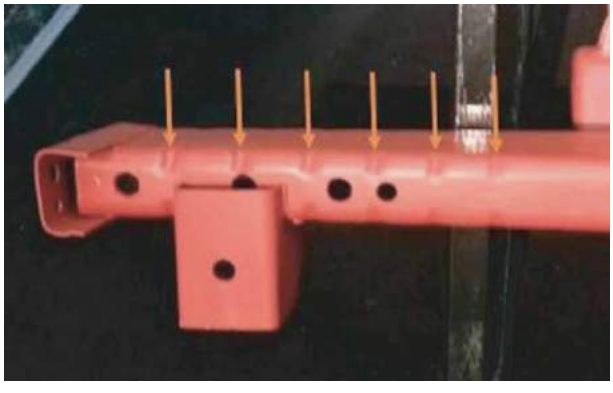

Figure 1. Collapse triggers example [12].

Witteman's doctoral dissertation [20] studies profile geometry and collapse trigger types among other subjects, chapter 3: "Numerical Design of Stable Energy Absorbing Longitudinal Members" analyses 8 different collapse triggers; bead, notch, spheres, plastic fold, smaller thickness, circular notch, circular holes and oval hole.

Witteman applied an incremental load to profiles with the different triggers causing them to yield and deform up to a 180 mm deflection, this way obtaining a force vs. deflection graph, from which the first force peak of each trigger usage and the overall energy absorbed after a 175 mm deflection were obtained. In this case the most relevant result is the force peak due to its direct relationship with the collapse trigger quality. If the trigger is effective the local weakening of the profile takes place with a smaller applied force.

Based on said principle the results obtained from the force vs. deflection graph provide an excellent idea of which is the best trigger, nonetheless, it is also very important to have a qualitative evaluation of the deformed profiles. A good trigger must provide a homogeneously propagated and frontally initiated deformation, this is why crash simulations were performed in order to observe the different profiles behavior.

Now, with quantitative and qualitative results Witteman concludes that the best collapse trigger is a "bead" type, therefore, all that is left to determine is the optimal depth of the trigger for a maximum energy absorption. Witteman reduced 5%, 10% and 15% the cross-sectional area of the profile with the amount of penetration the bead trigger has on the area, and, with new impact simulations for each of said percentages a force vs. deformation length graph was obtained.

Once again the first force peak and the overall energy absorption after a 175 mm deflection were obtained for each cross-sectional area reduction, but now looking for maximum energy absorption. Again a qualitative evaluation is desired, for which new crash simulations were executed.

This way, a conclusion is reached in which the best value for cross-sectional area reduction is 10% due to its homogeneous propagation, frontally initiated deformation and maximum energy absorption.

After studying Witteman's work it is evident that focusing this paper on finding the best collapse trigger would do nothing but redound and would not represent a significant contribution to knowledge, nevertheless, he did not study this optimal trigger deeply, therefore, this paper focuses on finding the exact geometry of the bead trigger, the amount of triggers needed for an optimal performance within imperfect impact cases, and the behavior variations with different materials.

3. Methodology

For the purpose and reach of this work, and, due to their outstanding precision, only computational tools were employed. The software used and their applications are listed below.

- Siemens NX 8.5® – Employed for virtually drawing the analyzed 3D geometry.
- Altair® HyperMesh® – Software used for the simplification and meshing of the studied geometry.
- RADIOSS® – Solver used for the FEM non-linear cases processing.
- Altair® HyperCrash® – Crash oriented pre-processing software in which the impact set-up was defined.
- Altair® HyperView® and HyperGraph® – Qualitative and quantitative results visualization software with which results from the simulations where obtained.

From the already drawn vehicle chassis, shown in Fig. 2, the region of interest was selected, this work focuses on frontal impact, therefore, the collapsible region of the chassis, shown in Fig. 3a., was isolated from the rest with the intention of reducing the size of the finite element mesh and, therefore, the computational cost. Also, knowing the interest region is symmetrical, focusing this work on the study of the longitudinal members, and due to the fact that only frontal impacts are being studied, a further simplification can be made in which only one longitudinal member is isolated for analysis as shown in Fig. 3b.

3.1. Impact model

After a study region has been isolated, an impact model, defining how the crash will be simulated, must be developed.

First a 3D model of the analyzed longitudinal member was modeled with NX 8.5®, said model was the 1 m long collapsible region of the longitudinal member, with a $4'' \times 4''$ cross-section and a 1.9 mm thickness, according to the real dimensional properties of the construction material.

With a 3D model created, now the meshing of the study object is possible, within HyperMesh® a "Midsurface" of the 3D model was obtained in order to work with 2D surfaces, this simplification is possible due to the constant and relatively small thickness of the object, with these surfaces, a 10 mm element 2D mesh is created, element size chosen due to its conventional use in automotive applications, also, a rigid element was created on the rear opening of the object, where a concentrated load will be applied. The mesh created and the rigid element are shown on Fig. 4.

The previous mesh file was imported into HyperCrash® where the crash conditions were determined and implemented.

First, virtual materials were created and assigned to the study object, these materials were defined with the Johnson Cook elasto-plastic model for A36 steel and 6061-T6 aluminum respectively. For all the simulations

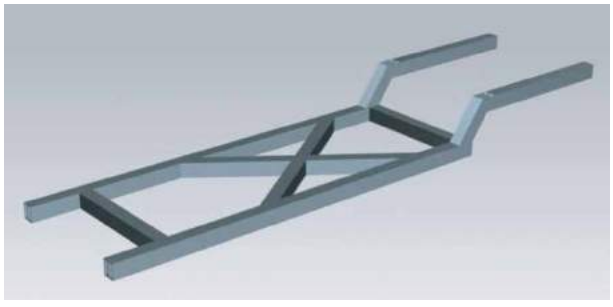

Figure 2. Analyzed chassis.

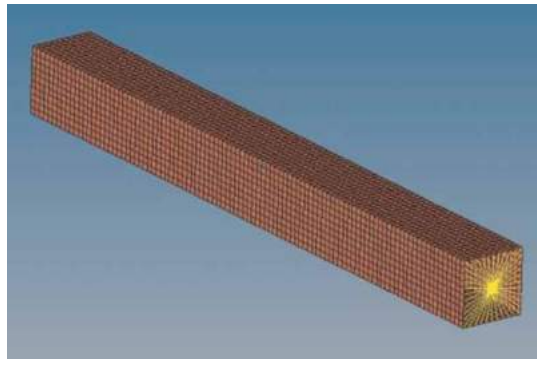

Figure 4. Meshed study object with rear rigid element.

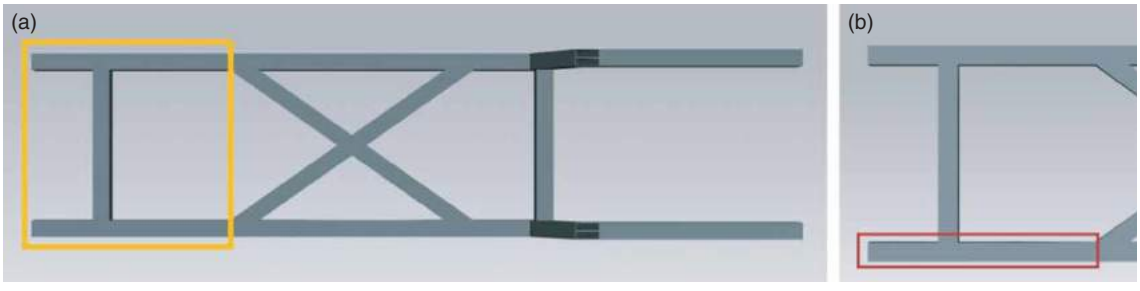

Figure 3. (a) Collapsible region of the analyzed chassis and (b) analyzed longitudinal member.

made along the work, the base units used were mm, kg and ms, therefore the software was provided with property values congruent with said units, for example, density was given in kg/mm^3. On Fig. 5 the materials properties given to the software are shown.

As a consequence of working with a 2D mesh, thickness must be defined, this is done through a "Shell" property with a 1.9 mm thickness according to the construction material.

Now, the previously mentioned concentrated load is created with the "added mass" tool, on the case shown a 534.052 kg mass is applied on the center node of the rigid element, this value represents the mass of the vehicle and the driver.

The creation of said "added mass" and the node where it is applied are shown on Fig. 6.

Since impact cases are being simulated, plastic deformations in the study object are expected, this means that contact conditions may take place and should be taken into consideration, therefore, a self-contact condition is applied to every node of the component with a 0.2 friction coefficient due to a metal-metal contact possibility.

Following the FMVSS No. 208 standard, an impact velocity of 35 MPH (15.646 mm/ms) is applied, for this, an imposed velocity is created with said value and applied on all the nodes of the component, this is done with a velocity vs. time function. Is important to mention that said imposed velocity should be present only during a small amount of time before the impact takes place, this because a realistic deceleration of the component is expected as a consequence of the impact. Taking this into account a start time of 0 ms and an end time of 0.01 ms are defined, being this enough to give the component the desired initial velocity before the first contact happens.

At this point the only object left to create is the one the component is crashing against, once again, following FMVSS No. 208 standard, a fixed rigid wall is created with a 1 mm gap from the component, said gap, for the previously created imposed velocity to be off when the first contact takes place. It is also important to know that

(a)

Choose Material Law

RADIOSS — Johnson-Cook (2)

Title	A36 STEEL
Initial density	7.85E-6
Reference density	0
Young modulus	200
Poisson ratio	.26
Yield stress	.286
Hardening param.	.5
Hardening exponent	.228
Failure plastic strain	1E30
Maximum stress	.4
Strain rate coeff	.0171
Reference strain rate	1

(b)

Choose Material Law

RADIOSS — Johnson-Cook (2)

Title	6061 ALUMINUM
Initial density	2.7E-6
Reference density	0
Young modulus	70
Poisson ratio	.33
Yield stress	.29
Hardening param.	.203
Hardening exponent	.35
Failure plastic strain	1E30
Maximum stress	.26
Strain rate coeff	.011
Reference strain rate	1

Figure 5. (a) Steel and (b) aluminum material properties given to the software.

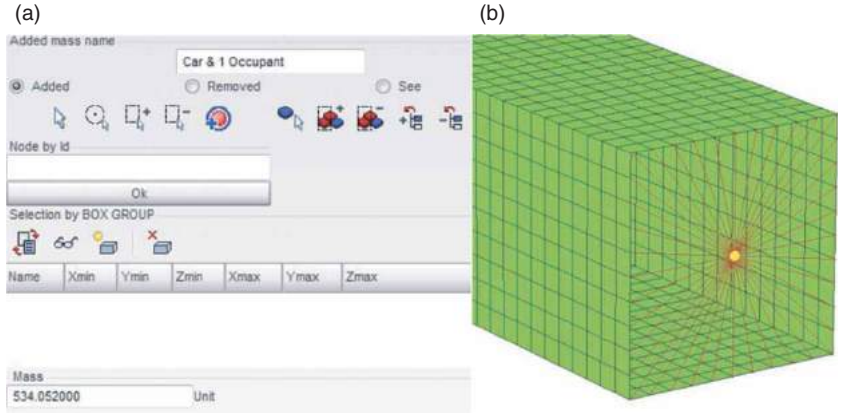

Figure 6. (a) Added mass properties and (b) application node.

crash wall was created taking 500 mm of slave nodes into consideration, this means that from the wall towards the component all the nodes inside a 500 mm volume may have contact with the impact wall. This distance may be freely defined, but always taking into account that if, any node outside said volume reaches the wall it will go straight through it, giving unreal results.

Another factor taken into consideration was defining the contact between the component and the wall as tied, this because the front of the vehicle will have a bumper, which restricts the longitudinal members translation, nevertheless a friction coefficient may be defined if the simulation is made with the bumper or if this factor is chosen to be neglected.

The fixed plane with the study object and slave nodes is shown on Fig. 7.

Finally, the simulation parameters are defined; 60 ms of collision will be simulated, the nodal time step is not defined, allowing the software to define the best one, an animation step is requested every 60μs looking for a total of 1000 steps in the whole simulation and historical data is requested every 90 ns. This parameter configuration is shown on Fig. 8.

This last step creates the necessary files for RADIOSS® to solve the finite element model, in average it takes 8 minutes to solve these models, afterwards it is possible to look at and analyze the results.

In order to look at qualitative results the .h3d generated file is read with HyperView®, and looking for quantitative results the generated file ended with T01 is interpreted by HyperGraph® where an absorbed energy vs. time graph can be generated. On Fig. 9, examples of these results are shown as close as possible to the 50 ms mark, instant chosen due to a 50% collapse having already happened on a perfectly frontal impact, and therefore, providing significant and representative data. This data acquisition instant is used on every experiment along the document.

The previous results were compared against those obtained by Witteman in his doctoral dissertation, which contain physical tests, and also, against those from the RD-3030 tutorial from Altair®. Comparisons which allowed to find similarities and congruencies, and therefore, validate the model used.

3.2. Experimentation method

The experimentation used along this work was designed based on Dr. Taguchi's robust design methodology [19], following said methodology we begin with the creation of the P diagram for the studied product. P diagram shown on Fig. 10.

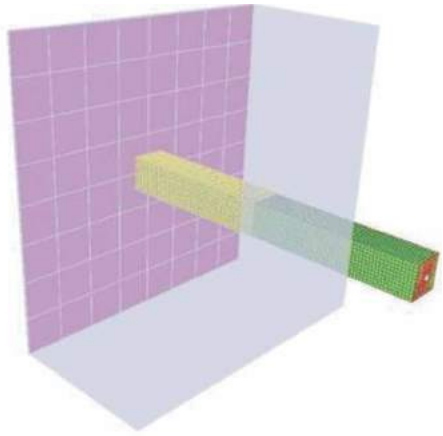

Figure 7. Impact wall with study object and slave nodes (in yellow).

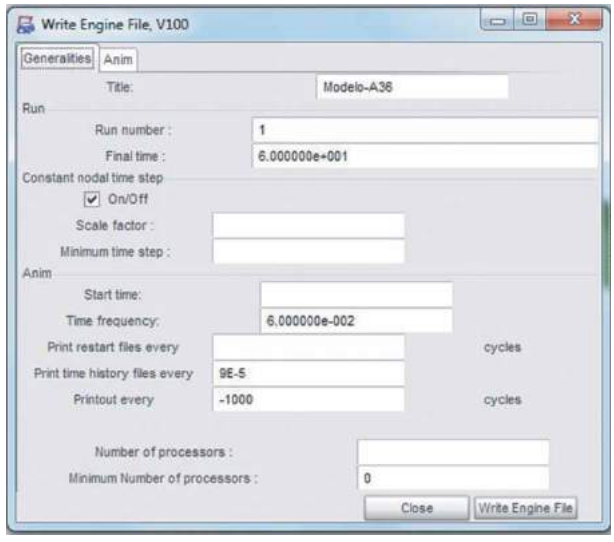

Figure 8. Simulation parameters definition.

The components of a P diagram are defined as follows:

Signals "M" – Signals are the input received by a product, for which a transformation is expected within the product itself. In this particular case the signal is the kinetic energy of the vehicle before the collision.

This being an ongoing project, certain constraints, are already defined.

In terms of mass, the vehicle must not exceed 1000 kg, and should be able to transport a maximum load of 400 kg (including occupants), knowing this and working under the FMVSS No. 208 parameters the following 4 cases were selected:

1. The vehicle crashes at 35 MPH with a single 80 kg occupant (M1).
2. The vehicle crashes at 35 MPH with two 80 kg occupants (M2).

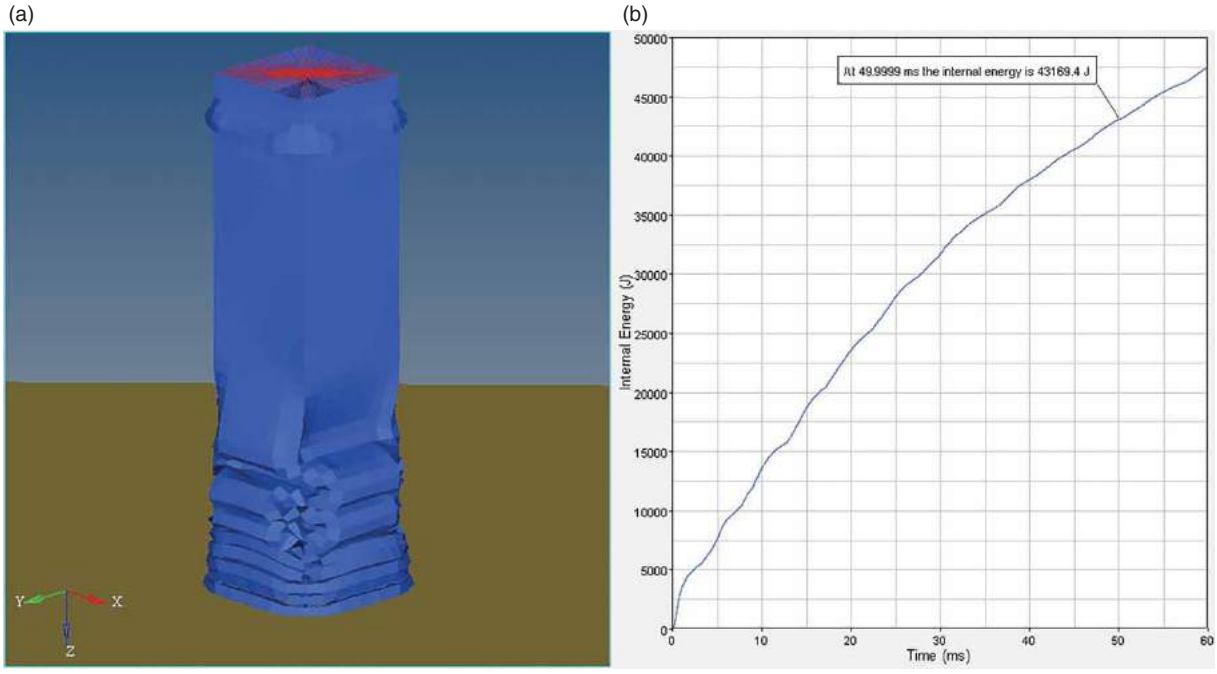

Figure 9. (a) Qualitative and (b) quantitative results of simulation example.

3. The vehicle crashes at 35 MPH with an 80 kg occupant and 200 kg in load (M3).
4. The vehicle crashes at 35 MPH with two 80 kg occupants and 200 kg in load (M4).

With the previous cases, the 4 different signals used in the experimentation are defined through the kinetic energy formula (Eq. 3–1).

$$E_k = \frac{1}{2}mv^2$$

Eq. 3–1: Kinetic energy
Where:
E_k : Kinetic energy (J)
m : Mass (kg)
v : Velocity (m/s)

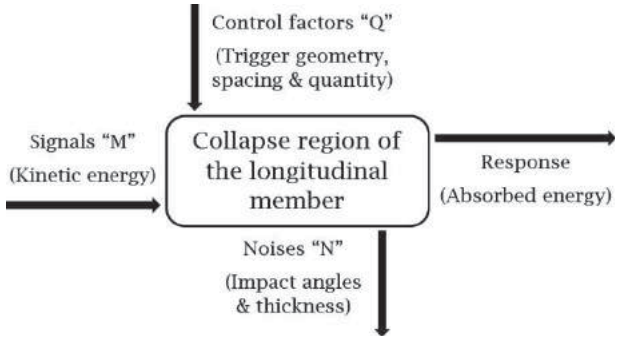

Figure 10. P diagram.

It is important to note that only half of the previously mentioned mass will be considered because only one of the longitudinal members is being simulated and a homogeneously distributed mass is assumed. The 4 signal values are shown on Tab. 1.

Finally, it is also important to mention that, the added mass used in the simulations is slightly different from the values previously mentioned due to the mass of the studied object being subtracted from the total mass, as it is automatically taken into account by the software.

Noise "N" – These are factors that cannot be controlled and may or may not be present, they are unpredictable and impact negatively on the performance of the product. On the study case, in order to consider real phenomenon present during a collision and the unavoidable variability of every manufacture process the following noises were chosen:

1. Dive angle – Caused by the driver's braking reaction before an imminent collision, braking causes the frontal suspension to compress and the rear to expand.

Table 1. Signal values.

Signal	Kinetic energy (J)
M1	66098.7
M2	70994.8
M3	78339.2
M4	83235.3

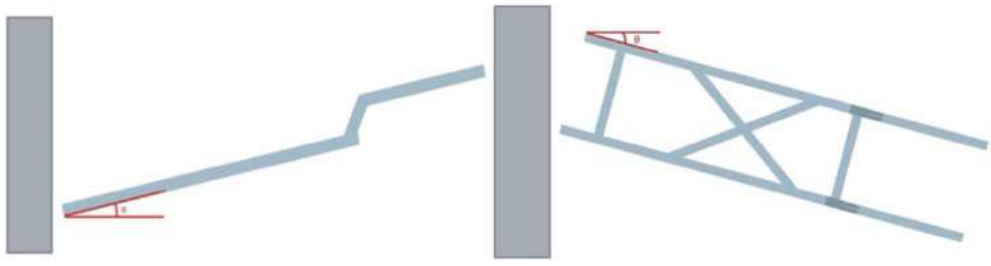

Figure 11. (a) Dive angle (side view) and (b) incidence angle (top view)

A dramatized illustration of this angle is shown on Fig. 11a. In this particular case, the suspension parameters are known, with them, a maximum dive angle of 3.633° was determined.

2. Incidence angle – Caused by the driver's reaction to steer away before an imminent collision.
   Fig 11b shows an illustration of this angle. Following FMVSS No. 208 standard and looking for the worst case scenario, a maximum incidence angle of 30° was chosen. A greater angle would catalog the collision as a side impact which is not studied within the range of this work.
3. Component thickness – A variation in this parameter is unavoidable due to the extrusion process through which the selected profile is manufactured. In this case a 0.1 mm reduction in the profile thickness is chosen because; a reduction would weaken the structure, and a 0.1 mm variation is an extreme variation value that represents a critical case.

With the noises defined and following Taguchi's method an L_4 orthogonal array is selected because only 2 levels will be possible for each noise (present or absent), therefore an L_4 array is ideal. Tab. 2 shows this array.

It is important to note that the way to arrange data is defined by the array itself, these arrays were statistically defined by Taguchi and are to be used as provided. The L_4 array gives 4 different noise configurations to be used in the experimentation.

Control factors "Q" – These factors are the parameters which the experimenter may tune in order to obtain the desired results.

Starting from the work done by Witteman we know that the best trigger is a "bead", nevertheless, he only obtains the ideal value for the depth, he does not provide the optimal dimensions, quantity or distance between implemented triggers. With this in mind the following factors were selected for control.

1. Trigger height
2. Trigger width
3. Distance between triggers
4. Quantity of triggers

For all the control factors 3 levels were chosen.

- For the height, 80, 60 and 40 mm, these because the profile edge is a high energy absorbent feature chosen to be left intact, and having a 10 mm element mesh means multiples of 10 mm variations allow mesh size conservation.
- For the width, 40, 30 and 20 mm, these due to the minimum width allowed by the mesh size being 20 mm and a chosen 10 mm increase.
- For the distance between triggers, 30, 20 and 10 mm also due to the minimum spacing of one element as a consecuence of the mesh size.
- For the quantity, 12, 8 and 4 triggers, this was determined with the maximum number of triggers of maximum width, that could fit along the studied longitudinal member.

With the previous information an L_9 orthogonal array was chosen because it is ideal for 4 factors with 3 levels each. This array is shown on Tab. 3. This array gives 9 different configurations for the control factors to be used in the experimentation. In order to illustrate in a better way the control factors used, on Fig. 12 the 9 configurations obtained from the array are shown.

It is important to mention that all the triggers were created with a direct modification of the midsurface mesh,

Table 2. L_4 orthogonal array for noises.

	Dive angle	Incidence angle	Thickness
N1	0°	0°	1.9
N2	0°	30°	1.8
N3	3.663°	0°	1.8
N4	3.663°	30°	1.9

Table 3. L_9 orthogonal array for control factors.

	Height	Width	Quantity	Spacing
Q1	80	40	12	30
Q2	80	30	8	20
Q3	80	20	4	10
Q4	60	40	8	10
Q5	60	30	4	30
Q6	60	20	12	20
Q7	40	40	4	20
Q8	40	30	12	10
Q9	40	20	8	30

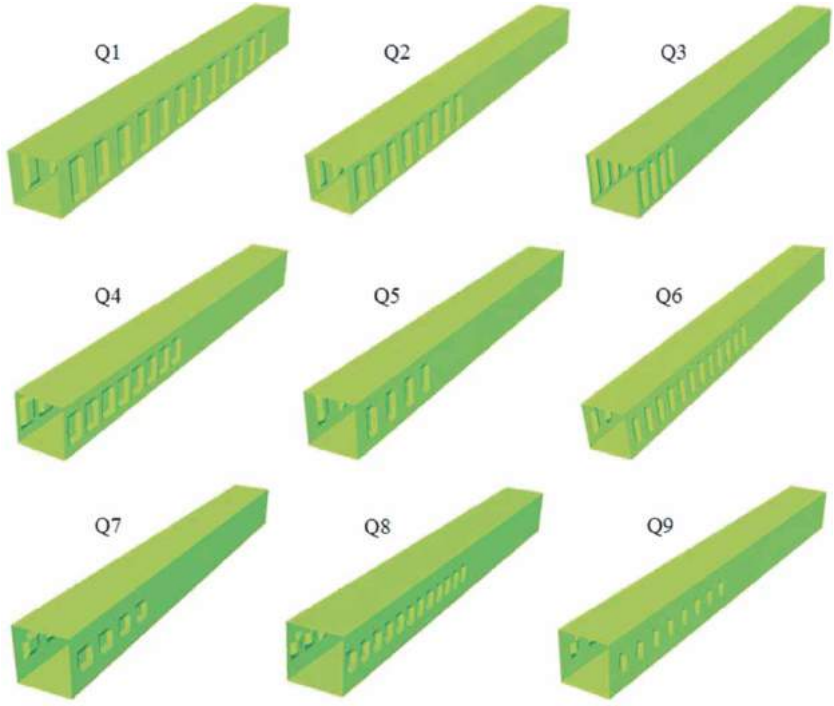

Figure 12. Control factors configurations.

with a depth of 4.885 mm, this value was determined following Witteman's method and a 10% reduction in the cross-section area.

Response – What is expected as an output, from a product.

In this case, energy absorption is expected. During a collision the kinetic energy from the vehicle is transformed into absorbed energy through the deformation of components.

Within our result analysis software it is possible to obtain a result called "internal energy" which is precisely the energy absorbed by the component during its deformation, therefore, this value is the response obtained during the experimentation.

With all the P diagram parts determined the only thing left to build is the table to be filled during the experimentation runs, said table is constructed following Taguchi's method and taking into account that we are working with a dynamic analysis. The table to be filled is Tab. 4, where all the # symbols represent an experimental result.

4. Experimentation and results

The previous table gives a total of 144 experimental runs to be executed, knowing that every simulation takes about 8 minutes to be solved, the total computational cost of the experimentation is 19.2 hours per material, therefore, taking into account this work was done with A36 steel and 6061-T6 aluminum, a total of 38.4 hours of computational cost were needed.

Due to the previously mentioned computational cost the use of 24 simultaneous computers was chosen with

Table 4. Experimentation table.

	M1				M2				M3				M4			
Experiment	N1	N2	N3	N4	N1	N2	N3	N4	N1	N2	N3	N4	N1	N2	N3	N4
Q1	#	#	#	#	#	#	#	#	#	#	#	#	#	#	#	#
Q2	#	#	#	#	#	#	#	#	#	#	#	#	#	#	#	#
Q3	#	#	#	#	#	#	#	#	#	#	#	#	#	#	#	#
Q4	#	#	#	#	#	#	#	#	#	#	#	#	#	#	#	#
Q5	#	#	#	#	#	#	#	#	#	#	#	#	#	#	#	#
Q6	#	#	#	#	#	#	#	#	#	#	#	#	#	#	#	#
Q7	#	#	#	#	#	#	#	#	#	#	#	#	#	#	#	#
Q8	#	#	#	#	#	#	#	#	#	#	#	#	#	#	#	#
Q9	#	#	#	#	#	#	#	#	#	#	#	#	#	#	#	#

Table 5. Experimentation results for A36 steel inputs M1 & M2.

A36	M1				M2			
Experiment	N1	N2	N3	N4	N1	N2	N3	N4
Q1	40524.6	23630.9	38909.8	25832.8	41143.2	23735.5	39597.4	25840.1
Q2	39651.9	25239.7	38329.4	28782.8	40375.5	25358.7	38795.3	28883.4
Q3	37983.9	22951.8	35185	24127.1	38500.2	23302.7	35519.6	24175.4
Q4	40149	23179.1	36358.3	25915.8	40680.5	23161.8	37082.9	26327.7
Q5	37570.6	24839.9	36166	25698.4	37614.7	24862.7	36766.1	25844.5
Q6	37690.4	25724.3	35781.5	25911.3	38392.7	25676.4	36424.4	26307.7
Q7	37471.9	24038	34665.2	26203.8	38751.3	24103.8	35239.5	26336.9
Q8	38991.3	24259.2	35671.2	25327.1	39377.5	24101.1	36345.9	25385.3
Q9	38219.4	25176.8	35634	26470	38625.4	25337.1	36317.5	26614.7

Table 6. Experimentation results for A36 steel inputs M3 & M4.

A36	M3				M4			
Experiment	N1	N2	N3	N4	N1	N2	N3	N4
Q1	42127.8	23690.6	40426.1	25760.3	42542	23967.7	40876.5	25967.7
Q2	41098.8	25319.5	39709.1	29112	41254.9	25627.9	40135.7	29170.1
Q3	39296.3	23599.5	36076.1	24158.6	39693.1	23706.9	36469.5	24219.4
Q4	41720.6	23266.6	38067.4	26211	42161.1	23251.5	38417.8	26272.2
Q5	39026.7	24933.3	37618.4	26012.6	39735.7	25024.9	38225.4	26083.4
Q6	39078.7	25801.3	36934.2	26155.5	39702.5	25658.9	37289.4	26118.9
Q7	39455.3	24453.4	35904.9	26609.2	39964.7	24783	36363.5	26734.8
Q8	40329.5	24359.1	37372.6	25716.8	41134.4	24603.7	37720.6	25831.1
Q9	39850.6	25526.2	37146.7	26681.7	40238.2	25612.2	37548.9	26822.1

Table 7. Experimentation results for 6061-T6 aluminum inputs M1 & M2.

6061-T6	M1				M2			
Experiment	N1	N2	N3	N4	N1	N2	N3	N4
Q1	28069.1	15455.1	24661.6	15919.1	28350.9	15535.3	23709	16434.9
Q2	27034.2	14318.5	24654.9	17008.1	27337.5	14816.1	24702.8	17023.2
Q3	25030.9	13108.3	23329	15696.2	24938.6	13017.4	23447.9	15683.4
Q4	25788.9	13296.9	23589.8	15931.2	26090.5	13341.4	23790.1	15952.3
Q5	25941.2	14471.9	22537.7	15545.1	26119.3	14512.7	22781	15605.8
Q6	26389.9	15770.2	23301.9	16921.4	26396.4	15850.7	23560.8	16952.3
Q7	26206.9	15075.9	23473	16251.8	26102.9	15096.3	23434	16304
Q8	26321.4	12542.9	23215.9	15203.2	26300.3	12687.8	23637.6	15127.8
Q9	25136	14986.2	23132.5	16871.1	25267.3	14992.8	23415.9	16906

Table 8. Experimentation results for 6061-T6 aluminum inputs M3 & M4.

6061-T6	M3				M4			
Experiment	N1	N2	N3	N4	N1	N2	N3	N4
Q1	28300.3	15138.5	22466	16162.1	29262.7	15864.7	24289.3	16220
Q2	27432.4	14760.6	25345.9	17018.7	27566.1	14878.4	25204.5	17002
Q3	25351.4	13216	23745.8	15812.5	25541.3	13282	23823.6	15695.5
Q4	25952.4	13332.7	24209.1	16090.9	26449.1	13280.7	24240.1	16081.5
Q5	26372.8	14850.6	22991.1	16305.7	26582.5	14532.9	23204.5	15669.1
Q6	26994.4	15663.9	23695.2	16898	27619.3	15731.4	23888.3	17056.4
Q7	26284.4	15204.6	23578.7	16318.4	26559.8	15107.5	23832.8	16245.7
Q8	26735.9	12716.3	23854.8	15330.8	26554.3	12622.8	24025.9	15417.6
Q9	25620.7	15078.1	23683.8	16923.8	25709	14565.6	23836.5	16882.3

which the effective experimentation time was reduced to 1 hour and 36 minutes.

The experimentation results for A36 steel are shown on Tab. 5 for inputs M1 and M2 and on Tab. 6 for inputs M3 and M4. For 6061-T6 aluminum the results are shown on Tab. 7 for inputs M1 and M2 and on Tab. 8 for inputs M3 and M4.

With the previous results obtained from the experimentation process an analysis and interpretation must be made. This is mainly done with two post-experimentation results; signal to noise ratio (S/N) and efficiency (β).

The signal to noise ratio (S/N) condenses various results into a single one which shows the amount of

variation present in the data, the performance, and how is it affected by the noises. A higher S/N means a higher performance and therefore a highly robust product.

For dynamic cases, like the one under study, S/N is calculated with Eq. 4–1 shown below.

$$\frac{S}{N} = 10\log\left(\frac{1}{r} * \frac{S_\beta}{Ve}\right)$$

Eq. 4–1: S/N for dynamic cases

Where:

r : Signals sum of squares

S_β : Signals and responses sum of products, squared and divided by r

Ve : Responses sum of squares minus S_β and divided by the amount of responses

The graph shown on Fig. 13 represents S/N, on it, the input signals (x axis) are related with the response (y axis). The dispersion of every input signal is the variability (represented with the Greek letter σ), greater variability means greater influence of noises.

The efficiency ($\boldsymbol{\beta}$) represents the relationship between the input signals and the response. A greater β means better energy conversion, in other words, a greater amount of the input energy is transformed into useful output energy.

$\boldsymbol{\beta}$ is calculated as the input signals, and, responses sum of products divided by r.

Where:

r : Signals sum of squares

On the graph displayed in Fig. 14, $\boldsymbol{\beta}$ is the slope of the line that best adjust the relationship between the input signals (x axis) and the response (y axis). A bigger slope translates as better energy conversion.

Analyzing the results of S/N and $\boldsymbol{\beta}$ for each of the experiments allows us to determine how every control factor affects the response and therefore obtain the best configurations.

From the results shown on Tab. 5, 6, 7 and 8, the values of S/N and $\boldsymbol{\beta}$ were calculated for both materials under study, these values are shown on Tab. 9 for A36 steel and on Tab. 10 for 6061-T6 aluminum.

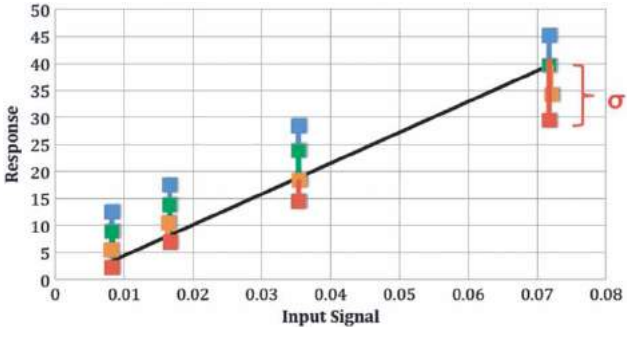

Figure 13. Graphic representation of S/N.

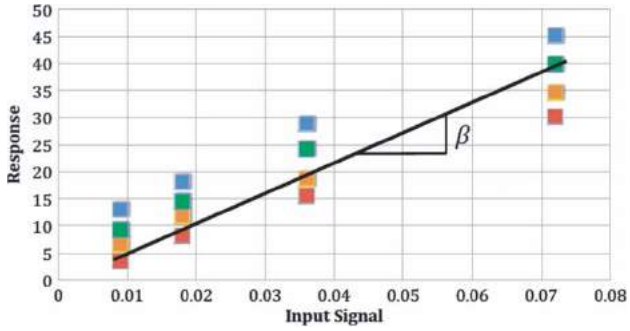

Figure 14. Graphic representation of β.

Table 9. S/N and β results for A36 steel.

A36 Experiment	Control Factors			Results		
	Height	Width	Quantity	Spacing	S/N	β
Q1	1	1	1	1	-86	0.436
Q2	1	2	2	2	–84.2	0.446
Q3	1	3	3	3	–85.3	0.407
Q4	2	1	2	3	–85.6	0.426
Q5	2	2	3	1	–84.3	0.421
Q6	2	3	1	2	–83.9	0.423
Q7	3	1	3	2	–84.1	0.417
Q8	3	2	1	3	–84.9	0.421
Q9	3	3	2	1	–84	0.426

Note that only the control factors levels are shown (not their correspondent values) for analysis and simplification purposes.

With the previous information an average value for each level of every factor is obtained, finding the factor's influence on each of the results, with this, the ideal level of the factors was found in order to maximize S/N and $\boldsymbol{\beta}$.

On the following figures the above mentioned averages are shown with the best level for every factor highlighted in green. Fig. 15 and 16 for A36 steel and Fig. 17 and 18 for 6061-T6 aluminum.

From the previous results of A36 steel we find that in order to maximize S/N the combination would be A3, B3, C3 and D2, nevertheless, in order to maximize $\boldsymbol{\beta}$ the combination would be A1, B2, C2 and D2.

Table 10. S/N and β results for 6061-T6 aluminum.

6061-T6 Experiment	Control Factors			Results		
	Height	Width	Quantity	Spacing	S/N	B
Q1	1	1	1	1	–86.5	0.279
Q2	1	2	2	2	–86.2	0.279
Q3	1	3	3	3	–86.6	0.258
Q4	2	1	2	3	–86.8	0.264
Q5	2	2	3	1	–86	0.264
Q6	2	3	1	2	–85.2	0.277
Q7	3	1	3	2	–85.7	0.27
Q8	3	2	1	3	–87.5	0.26
Q9	3	3	2	1	–85.2	0.268

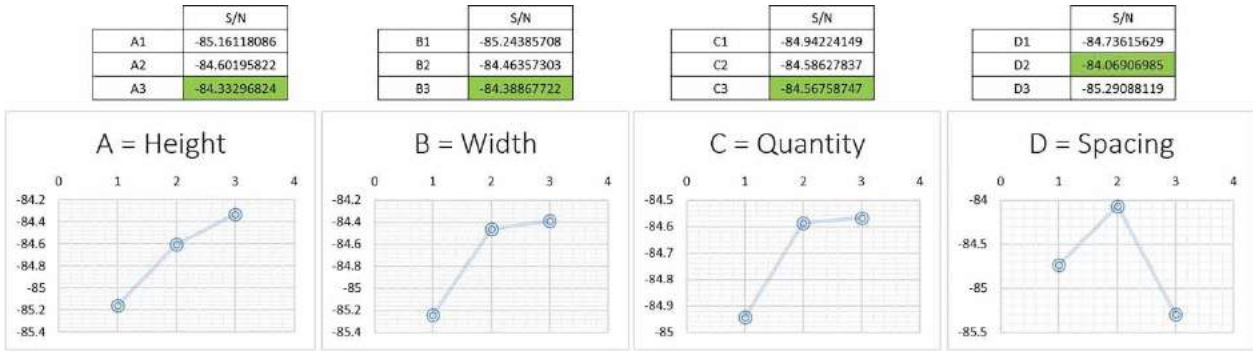

Figure 15. Control factors influence on S/N for A36 steel.

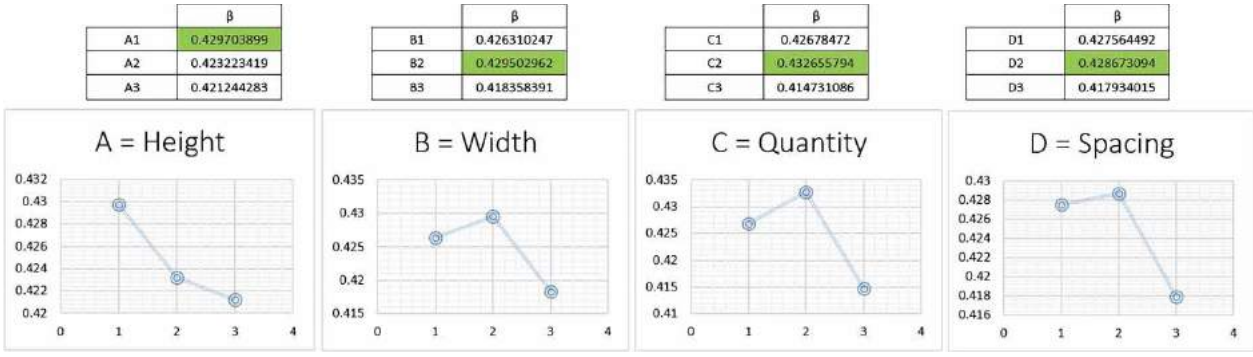

Figure 16. Control factors influence on β for A36 steel.

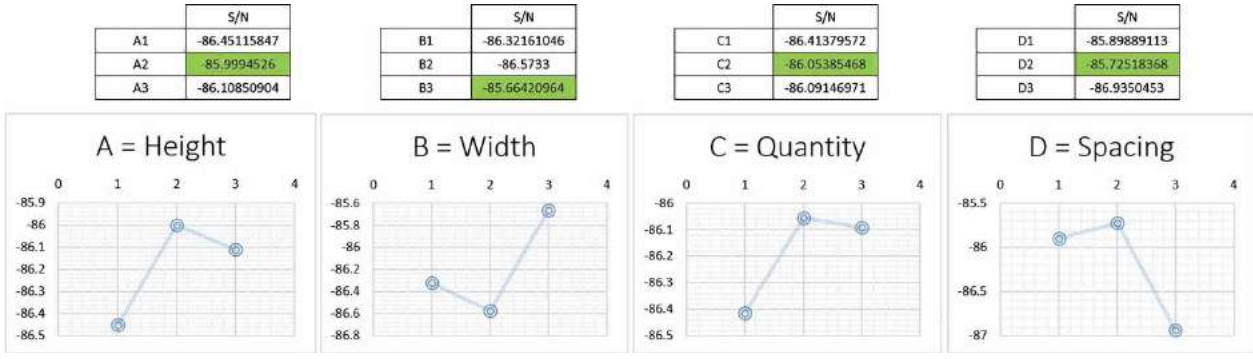

Figure 17. Control factors influence on S/N for 6061-T6 aluminum.

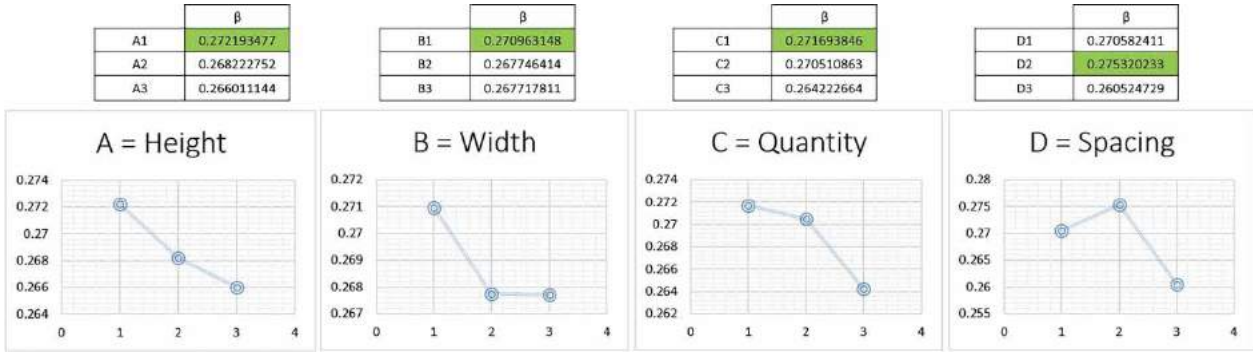

Figure 18. Control factors influence on β for 6061-T6 aluminum.

Table 11. Control factors influence percentages on S/N and β for A36 steel.

	S/N	β
A	21.7%	11.5%
B	27.3%	19.3%
C	5.4%	48.9%
D	45.6%	20.4%

Table 12. Control factors influence percentages on S/N and β for 6061-T6 aluminum.

	S/N	β
A	7.5%	11.3%
B	29.7%	4%
C	5.3%	18.6%
D	57.6%	66%

Clearly these combinations are not equal, therefore, in order to choose the best combination, the influence percentage each factor has on S/N & β was obtained. Said influence percentages are shown on Tab. 11.

From analyzing the previous table:

- Factor A has a greater influence on S/N therefore its ideal level is A3.
- Factor B has a greater influence on S/N therefore its ideal level is B3.
- Factor C has a greater influence on β therefore its ideal level is C2.
- Factor D has a greater influence on S/N therefore its ideal level is D2.

In conclusion, for A36 steel, the optimal combination is A3, B3, C2 and D2, which means that, in order to minimize the sensibility to noises and maximize the energy absorption, the collapsible region of the longitudinal member should have eight 40 mm high and 20 mm wide triggers with 20 mm in between. This configuration is shown on Fig. 19a.

Now, from the results of 6061-T6 aluminum, in order to maximize S/N the combination would be A2, B3, C2 and D2, and for maximizing β the combination would be A1, B1, C1 and D2.

Once again these combinations are not equal and finding the influence percentages of each factor on S/N & β is needed. Tab. 12 shows these percentages.

From analyzing the previous table:

- Factor A has a greater influence on β therefore its ideal level is A1.
- Factor B has a greater influence on S/N therefore its ideal level is B3. Factor C has a greater influence on β therefore its ideal level is C1.
- Factor D has a greater influence on β therefore its ideal level is D2.

Meaning that, for 6061-T6 aluminum, the optimal combination is A1, B3, C1 and D2, therefore, in order to minimize the influence of noises and maximize the energy absorption, the collapsible region of the longitudinal member should have twelve 80 mm high and 20 mm wide triggers with 20 mm in between. Fig. 19b shows this configuration.

In order to verify that the optimal configurations are truly optimal they must be tested with the experimentation method. The results for A36 steel are shown on Tab. 13 for inputs M1 and M2 and on Tab. 14 for inputs M3 and M4, for 6061-T6 aluminum the results for inputs M1 and M2 are found on Tab. 15 and for inputs M3 and M4 on Tab. 16.

One more time values for S/N and β are calculated, these are shown on Tab. 17 for A36 steel and on Tab. 18 for 6061-T6 aluminum.

Analyzing the previous results, for A36 steel a higher S/N than on any other experiment was found, as a consecuence, it is safe to say that the optimal configuration is truly optimal and the work objective is fulfilled. Talking about β, despite not a maximum value was obtained because the influence percentages analysis favored S/N, a satisfactory above average value was obtained.

For 6061-T6 aluminum a higher β than on any other experiment was found, therefore, it is safe to say that the

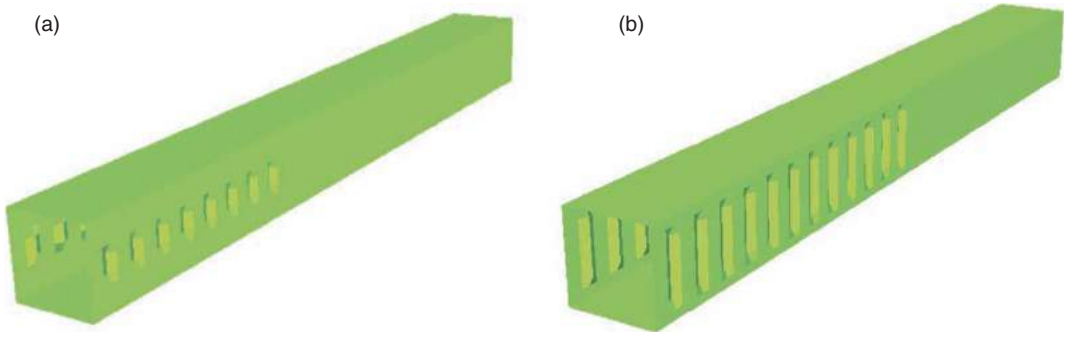

Figure 19. Optimal configuration of the study object with (a) A36 steel and (b) 6061-T6 aluminum.

Table 13. Experimentation results for A36 steel inputs M1 & M2 with optimal configuration.

A36 Experiment	M1				M2			
	N1	N2	N3	N4	N1	N2	N3	N4
Qo	37935.9	25296.4	36115.8	26899.3	38696.1	25528	36814.3	27098.4

Table 14. Experimentation results for A36 steel inputs M3 & M4 with optimal configuration.

A36 Experiment	M3				M4			
	N1	N2	N3	N4	N1	N2	N3	N4
Qo	39615.1	25754.9	37440.7	27297.1	39671.1	25816.7	37653.3	27408.4

Table 15. Experimentation results for 6061-T6 aluminum inputs M1 & M2 with optimal configuration.

6061-T6 Experiment	M1				M2			
	N1	N2	N3	N4	N1	N2	N3	N4
Qo	26341.4	15791	24135.1	17184.5	26636.5	15694.3	24306.3	17279.4

Table 16. Experimentation results for 6061-T6 aluminum inputs M3 & M4 with optimal configuration.

6061-T6 Experiment	M3				M4			
	N1	N2	N3	N4	N1	N2	N3	N4
Qo	27027.8	15789.8	24407.9	17457.2	27103.3	15414	24877.3	17474.3

Table 17. S/N and β results for A36 steel with optimal configuration.

A36 Experiment	Control Factors				Results	
	Height	Width	Quantity	Spacing	S/N	β
Qo	3	3	2	2	–83.7	0.43

Table 18. S/N and β results for 6061-T6 with optimal configuration.

6061-T6 Experiment	Control Factors				Results	
	Height	Width	Quantity	Spacing	S/N	β
Qo	1	3	1	2	–85.3	0.28

optimal configuration is truly optimal and, once again, the work objective is fulfilled. On this case β was mostly favored by the influence percentages analysis, which is why not a maximum S/N value was obtained, nevertheless the best possible value was found.

Finally a last experiment was executed with Witteman's configuration, in this, a single bead trigger is implemented with the maximum possible height and minimum possible width, a height of 90 mm and a width of 20 mm were these values for our study object. Fig. 20 shows this configuration.

This configuration was tested with the experimental method using A36 steel and 6061-T6 aluminum. The results for A36 steel are shown on Tab. 19 for inputs M1 and M2 and on Tab. 20 for inputs M3 and M4, for 6061-T6 aluminum the results for inputs M1 and M2 are found on Tab. 21 and for inputs M3 and M4 on Tab. 22.

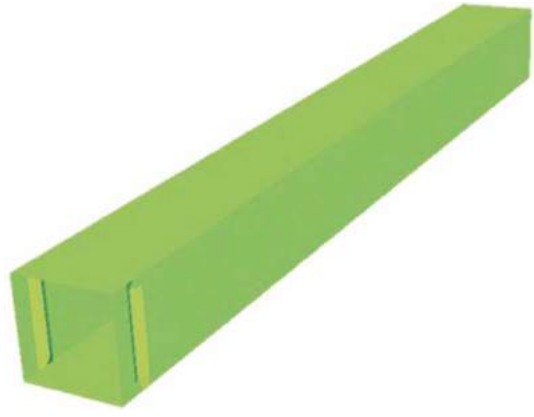

Figure 20. Witteman's configuration of the longitudinal member.

With the previous results, values for S/N and β are obtained once more. These values are shown on Tab. 23 for A36 steel and on Tab. 24 for 6061-T6 aluminum.

Comparing the S/N and β values from the optimal configuration with the ones from Witteman's configurations, we conclude that the optimal configurations found have lesser variability caused by noises and greater energy absorption.

With A36 steel a 16.33% variability reduction and a 1.88% energy absorption increase were obtained, and with 6061-T6 aluminum a 3.87% variability reduction and a 1.8% energy absorption increase were obtained. Proving the optimal configurations results to be better than those obtained with Witeman's model.

Table 19. Experimentation results for A36 steel inputs M1 & M2 with Witteman's configuration.

A36 Experiment	M1				M2			
	N1	N2	N3	N4	N1	N2	N3	N4
Qw	37474.9	22608.8	35354.7	25120.6	38795.7	22692.9	35965.8	25240.9

Table 20. Experimentation results for A36 steel inputs M3 & M4 with Witteman's configuration.

A36 Experiment	M3				M4			
	N1	N2	N3	N4	N1	N2	N3	N4
Qw	38910.9	22877.6	36644	25362.5	39925.5	22817.1	37176.6	25374.2

Table 21. Experimentation results for 6061-T6 aluminum inputs M1 & M2 with Witteman's configuration.

6061-T6 Experiment	M1				M2			
	N1	N2	N3	N4	N1	N2	N3	N4
Qw	24919.7	14421.6	23136.7	15930.8	24925.3	14527.3	23430.4	15997.6

Table 22. Experimentation results for 6061-T6 aluminum inputs M3 & M4 with Witteman's configuration.

6061-T6 Experiment	M3				M4			
	N1	N2	N3	N4	N1	N2	N3	N4
Qw	24698	14645.8	23494.6	15912.6	25106.2	14673.5	23852.4	15701.2

Table 23. S/N and β results for A36 steel with Witteman's configuration.

A36 Experiment	Control Factors				Results	
	Height	Width	Quantity	Spacing	S/N	β
Qw	NA	NA	NA	NA	–85.2	0.41

Table 24. S/N and β results for 6061-T6 with Witteman's configuration.

6061-T6 Experiment	Control Factors				Results	
	Height	Width	Quantity	Spacing	S/N	β
Qw	NA	NA	NA	NA	–85.6	0.26

5. Conclusions

Evidently, safety is an essential area within the automotive industry, without a doubt it will continue to be studied and perfected as long as collisions and unforeseen events keep on happening, fortunately technological advancement is allowing much more precise and affordable studies. With the help of computational tools, such as the ones used along this work, the amount of physical prototypes and tests have been significantly reduced as well as the expense and time needed for such studies.

An important conclusion of this work is that it is possible to improve, in a very significant amount, the behavior of a structure without changing the materials or the general geometry. On this case, simply by adding the proper configuration of collapse triggers 16.33% for A36 steel and 3.87% for 6061-T6 aluminum variability reductions were obtained, as well as 1.88% and 1.8% increases in eficiency respectively.

It is also important to mention that, the behavior of a structure during an impact situation does not depend exclusively on the geometry but on the material as well, which is why different trigger optimal configurations were obtained with A36 steel and 6061-T6 aluminum.

Using Taguchi's method proves the great advantage a preventive culture has over a corrective one. In this case not a single physical prototype was destroyed but the product to be build has been already optimized with the use of simulation tools and experimentation methods.

This work contributes to knowledge as it considers rarely evaluated but frequently present noise factors, uses an efficient and reliable optimization method and provides a new and flexible methodology capable of being applied to any chassis optimization, hopefully it will be used by chassis developers and crash analysts as a reliable and efficient tool.

Acknowledgements

The financial support in terms of scholarships and tuitions that the Instituto Tecnológico y de Estudios Superiores de Monterrey and CONACyT provided to the first author are hereby gratefully acknowledged.

The authors also greatly appreciate the tools provided by the Instituto Tecnológico y de Estudios Superiores de Monterrey Campus Toluca, without which, this work would not have been possible.

ORCID

Augusto Millán Gardea http://orcid.org/0000-0002-8751-8130
José Carlos Miranda Valenzuela http://orcid.org/0000-0003-4138-1551

References

[1] Abbasi, M.; Kazemi, R.; Ghafari Nazari, A.: Using Parametric Method for Investigating Automotive Chrashworthiness, International Journal of Automotive Engineering, 2011.
[2] Abbasi, M.; Ghafari Nazari, A.; Reddy, S.; Fard, M.: A new approach for optimizing automotive crashworthiness: concurrent usage of ANFIS and Taguchi method, Springer-Verlag, Berlin, 2013.
[3] Cantor, B.; Grant, P.; Johnson, C.: Automotive Engineering: Lightweight, Functional and Novel Materials, Taylor & Francis, New York, 2008. http://dx.doi.org/10.1201/9781420011906
[4] Christensen, J.: Lightweight hybrid electrical vehicle structural topology optimisation investigation focusing on crashworthiness, International Journal of Vehicle Structures & Systems, London, 2011.
[5] Ehsani, M.; Gao, Y.; Emandi, A.: Modern Electric, Hybrid Electric and Fuel Cell Vehicles: Fundamentals, Theory, and Design, Taylor & Francis, Florida, 2010.
[6] Erjavec, J.: Automotive Technology A Systems Approach, Delmar Learning, New York, 2005.
[7] Fish, J.: AL 6061-T6 - Elastomer Impact Simulations, Massachusetts Institute of Technology, Massachusetts, 2005.
[8] Forsberg, J.: Topology optimization in crashworthiness design, 2006.
[9] Halderman, J.D.; Martin, T.: Hybrid and Alternative Fuel Vehicles, Pearson Prentice Hall, New Jersey, 2009.
[10] Huang, X.: Topology optimization of energy-absorbing structures, Taylor & Francis, Melbourne, 2007.
[11] Husain, I.: Electric and Hybrid Vehicles: Design Fundamentals, Taylor & Francis, Florida, 2010.
[12] Metalsa. 2025 Chassis design, Monterrey, 2014.
[13] Milliken, W.F.; Milliken, D. L.: Chassis Design: Principles and Analysis, Society of Automotive Engineers, Massachusetts, 2002.
[14] Murray, M.; Miranda, J. C.: Design For Six Sigma, Tecnológico de Monterrey, Toluca, 2014.
[15] Phadke, M. S.: Quality Engineering Using Robust Design, Prentice-Hall, New Jersey, 1989.
[16] Ross, P. Taguchi Techniques for Quality Engineering, McGraw-Hill, New York, 1996.
[17] Schumacher, A.: Parameter-based topology optimization for crashworthiness structures, University of Applied Science, Hamburg, 2005.
[18] Schwer, L.: Optional Strain-Rate Forms for the Johnson Cook Constitutive Model and the Role of the parameter Epsilon_0, Schwer Engineering & Consulting Services, Windsor, 2007.
[19] Taguchi, G.: Taguchi's Quality Engineering Handbook, John Wiley & Sons, Inc., New Jersey, 2005.
[20] Witteman, W.: Improved Vehicle Crashworthiness Design by Control of the Different Collision Situations, Technische Universiteit Eindhoven, Eindhoven, 1999.
[21] World Heath Organization. Mortality: Road traffic deaths by country. 2010. http://www.who.int/.
[22] Wu, Y.; Wu, A.: Taguchi Methods for Robust Design, The American Society of Mechanical Engineers, New York, 2000.